Journal of Nanomedicine & Nanotechnology
ISSN: 2157-7439
OPEN ACCESS Freely available online
Review Article

Metallic nanomaterials in cancer theranostics: A review of Iron oxide and Gold-based nanomaterials

Mehrnaz Mostafavi[1]*, Jalaledin Ghanavi[2], Mahtab Shaabani[3], Hamed Asadi[4] and Mahsa Alizadeh[5]

[1]Department of physics, Faculty of Paramedical Sciences, Shahid Beheshti University of Medical Sciences, Tehran, Iran; [2]MRC, NRITLD, Shahid Beheshti University of Medical Sciences, Tehran, Iran; [3]Department of internal medicine, Loghman hakim Hospital, Shahid Beheshti University of Medical Sciences, Tehran, Iran; [4]Department of internal medicine, Loghman hakim Hospital, Shahid Beheshti University of Medical Sciences, Tehran, Iran; [5]Department of physics, Faculty of Paramedical Sciences, Shahid Beheshti University of Medical Sciences, Tehran, Iran

ABSTRACT

The role of nanotechnology in cancer treatment and diagnosis, especially in the creation of new generation cancer diagnostic and therapeutic instruments, has attracted a lot of attention in recent years. Attempts to incorporate therapeutic and diagnostic properties in a single efficient nanomedicine solution have been made in large numbers. This concept, coined "theranostics," is a smart nanosystem capable of diagnosing, successful dissemination, and therapeutic reaction tracking. By integrating clinical functionality with molecular imaging, therapeutic interventions can be useful in the selection of medication, treatment preparation, objective response control and follow-up planning based on the specific molecular characteristics of the disorder. Here, we summarize a number of recent efforts in this regard and demonstrate that therapeutic systems and techniques have considerable potential for tracking and optimizing nanomedicine-mediated drugtargeting.

Keywords: Theranostic; Nanomedicine; Drug targeting; Iron oxide; Gold-based nanomaterials

INTRODUCTION

Metal nanoparticles have become increasingly popular in bioapplications such as biophysical studies, imaging, medical diagnostics, and cancer therapy in recent years [1]. Nanoparticles' nanoscale measurements allow them to easily combine with biological systems of similar size [2]. It means they can pass across biological membranes and communicate with biomolecules closely. These interactions can occur in magnetic materials (e.g. ⍺-fe2o3, Fe3o4, iron), and dielectric containment of gold and silver[3], in the form of NPs, which may have different physical conduct, including super paramagnetic behaviors. The therapeutic and diagnostic practical nanoparticles include a range of properties such as: target tissue disease, the transport of imaging agents for screening, the development of several therapeutic drinks, protection and biodegrade with non-toxic substances [4]. The clinical concern includes adverse effects of systemic chemotherapy administration [5-6], chemical therapeutical resistance [7] and reduced levels of chemotherapy agents in systemic tumor sites [6]. In this review paper, we are indeed interested in discussing the difficulties and opportunities of this emerging technology because of the value of integrating pictorial, targeting, and therapeutic agents in a single vehicle. iron oxide nanoparticles have the dual capacity to act as both magnetic and photothermal agents. In cancer cells, the laser excitation restores the optimal efficiency of magnetic hyperthermia, otherwise inhibited by intracellular confinement. In solid tumors in vitro, single-mode treatments reduced tumor growth, while DUAL-mode treatment resulted in complete tumor regression, mediated by heat-induced tumoral cell apoptosis and massive denaturation of the collagen fibers. Magnetic hyperthermia (MH) was used to treat a murine model of pancreatic cancer. Animals in which most of the nanoparticles remained in the tumor area after injection showed higher reductions in tumor volume growth. An inadequate body biodistribution of the particles after their intratumoral injection led to a decrease in the effectiveness of the MH treatment, the authors say. The authors suggest several factors that should be considered to improve the treatment effectiveness of Pancreatic cancer by magnetic hyperthermia [8].

Magnetic Fe_3O_4 NPs have shown great potential as an advanced platform because of their inherent magnetic resonance imaging (MRI), biocatalytic activity (nanozyme), magnetic hyperthermia treatment (MHT), photo-responsive therapy and drug delivery for chemotherapy and gene therapy. Small-size nanoparticles are

***Correspondence to**: Mehrnaz Mostafavi, Department of physics, Faculty of Paramedical Sciences, Shahid Beheshti University of Medical Sciences, Tehran, Iran, Tel: 989124766808, E-mail: mz_mostafavi@sbmu.ac.ir

Received: April 11, 2021; **Accepted**: April 21, 2021; **Published:** April 27, 2021

Citation: Mostafavi M, Ghanavi J, Shaabani M, Asadi H, Alizadeh M (2021) Metallic nanomaterials in cancer theranostics: A review of Iron oxide and Gold-based nanomaterials. J Nanomed Nanotech. 12: 564.

also desired due to the enhanced permeation and retention (EPR) effect. This review would provide a comprehensive reference for readers to understand the multifunctional Fe_3O_4 Nps in cancer diagnosis and treatment [9].

Properties of Iron oxide nanoparticles(IONPs) as theranostics agents

Another bioapplication for the area of cancer thermal and magnetic targeting is a specific developmental study of interested magnetic NP which are now being used as contrast agents for magnetic resonance imaging (MRI) [10-13]. Nanoparticles containing iron oxide (IONPs) are magnetite or hematite nanocrystals [14]. IONPs are a suitable alternative for theranostic agents among the broad range of nanoparticles. Strong magnetization and in vivo, minimal to no toxicities are important characteristics of IONP. In vitro research demonstrated that IONPs had accumulated in lysosomes, after integrating in the cells, where drug molecules are released due to low pH and proteases .If these Super paramagnetic iron oxide (SPIs) are affected by an external magnetic field, particles are sent to the target region and are handled locally for the drug [15].

Composite IONPs

IONPs are mainly used to diagnose diseases due to their intrinsic structure, but the integration of these particles and the optical properties of plasmon resonant particles increases the capabilities of these nanocomposites (NCs) in the analysis [16]. It is clear that the combination of these particles with gold nanoparticles (Au/Fe NCs) may be seen to increase the heat release many times more than Superparamagnetic iron oxide nanoparticles (SPIONs) alone. In addition, SPIONs should be coated with a polymer to maximize tumor aggregation and boost the thermalstability [17].

A Review of composite IONPs based theranosticagents

Iron–gold nanoparticles (N-isopropylacrylamide-co-methacrylic acid) are an example of an IONP application (PNIPAAmMA). The MPGNRs proposed a theranostic modal framework for cancer detection and treatment by integration of dual magnetic resonant resonance imaging and photoacoustic imaging (PAI) with a highly effective targeted PTT in a 2013 trial of Yang et al.

Figure1. (a) Schematic illustration of the synthesis and structure of MPGNRs. (b) TEM image of MPGNRs. Reprinted with permission from Ref [18].

The utilization of MPGNRs in tumor-bearing mice diagnosis (MRI diagnostic modality) has been documented in both the presence and absence of an external magnet. When magnetic targeting (0.4 T) was exposed for 36 hours, the most important changes in magnetic polymer-modified gold nanorods (MPGNRs) concentration at the tumor area (368 percent) were observed. They believed that MPGNRs did not sufficiently improve PA signals in tumor-bearing mice in the absence of magnetic targeting, as they did when the PAI was studied. In the presence of a magnetic targeting case, however, they discovered substantial contrast enhancement in PA scan images.

Finally, they were able to increase the contrast of the PA images by 3.7 times. In addition, the effectiveness of PAI was investigated in vitro. In this study, PA scan images from GNRs, PGNRs, and MPGNRs were compared in the presence and absence of an external magnet at various distances. Without the use of a magnet, PGNRS showed greater PA imaging contrast enhancement (2-fold) than GNRs. MPGNRs had the highest PA imaging contrast out of any of these particles. See (Figure 2). The PA signal was proportional to the concentration of particles (GNRs, PGNRs, and MPGNRs).

Figure 2a Schematic diagram of the experimental set-up for photoacoustic microscopy. (b) PA images in the phantom at different distances: GNRs (row 1), GNRs with MT (row 2) PGNRs (row 3), PGNRs with MT (row 4), MPGNRs (row 5), and MPGNRs with MT (row 6). Reprinted with permission from Ref [16].

The effectiveness of PTT was investigated in vitro, with C6 cells incubated with MPGNRs for 24 hours and a 900-Gauss magnetic field added to the cell culture. They did not notice any cell death after seeing Fluorescence micrographs, but the majority of cells died after being exposed to NIR light (wavelength 808 nm; 2 W/cm2) for 2 minutes. See (Figure 3a). Finally, the effectiveness of PTT was investigated in vivo using three classes of mice suffering from the same illness. The test mice were given 100 mL PBS intravenously and then exposed to NIR light (2 W/cm2) for 3 minutes. The second group was given PGNRs intravenously, then a magnet was added, and the animals were exposed to NIR radiation(PGNRs+ MT+NIR). The final group was studied in the same way as the first, with the exception that MPGNRs is injected intravenously (MPGNRs + MT+NIR). The temperature rises is associated (T=4.8°C, = 12.1°C, and 62.8°C, respectively). It means that in the most recent group trials, we increased temperature considerably more than in other care cases. See (Figures 3b & c). Furthermore, tumor development wasslowedfor10daysduringtreatment;thetumorvolumeonlyincreasedby(1137 ± 90 percent 915 ± 75 percent, and 284 ±79 percent, respectively) (Figure 3d) [18].

Figure 3a The fluorescence C6 cell micrographs were subjected to 24 h in lower left of the yellow line and were treated with MPGNRs. They were subjected to a 900-Gauss magnet field. Left: in front of radiation. Right: after radiation (808 nm for 2 min; green: live cells, red: dead cells). (b) Rise in temperature vs. time during irradiation. (c) The conversion of light absorption into heat by photothermal effect during irradiation for 3 min. (d) Quantitative study of the impact of different drugs on tumor size. Reprinted with the permission of Ref [18].

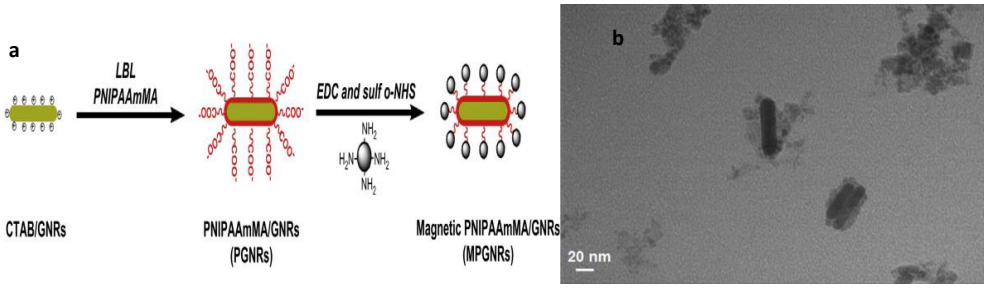

Figure 1: (a) Schematic illustration of the synthesis and structure of MPGNRs. (b) TEM image of MPGNRs. Reprinted with permission from Ref [18]

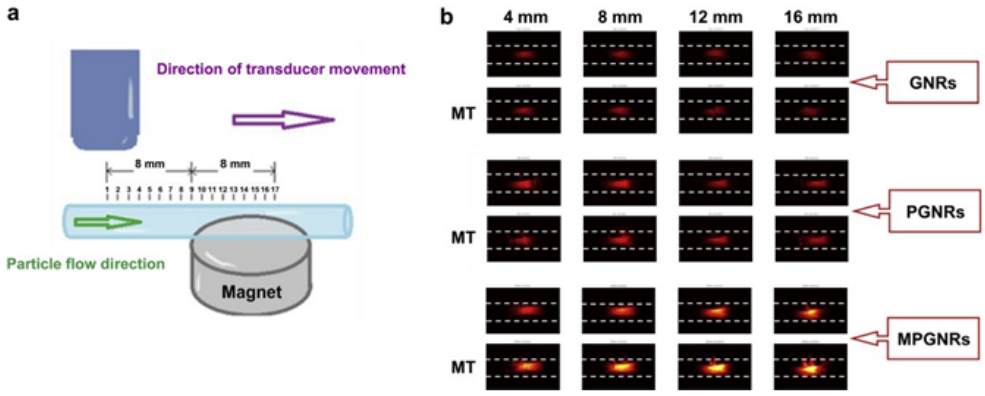

Figure 2: (a) Schematic diagram of the experimental set-up for photoacoustic microscopy. (b) PA images in the phantom at different distances: GNRs (row 1), GNRs with MT (row 2) PGNRs (row 3), PGNRs with MT (row 4), MPGNRs (row 5), and MPGNRs with MT (row 6). Reprinted with permission from Ref [16].

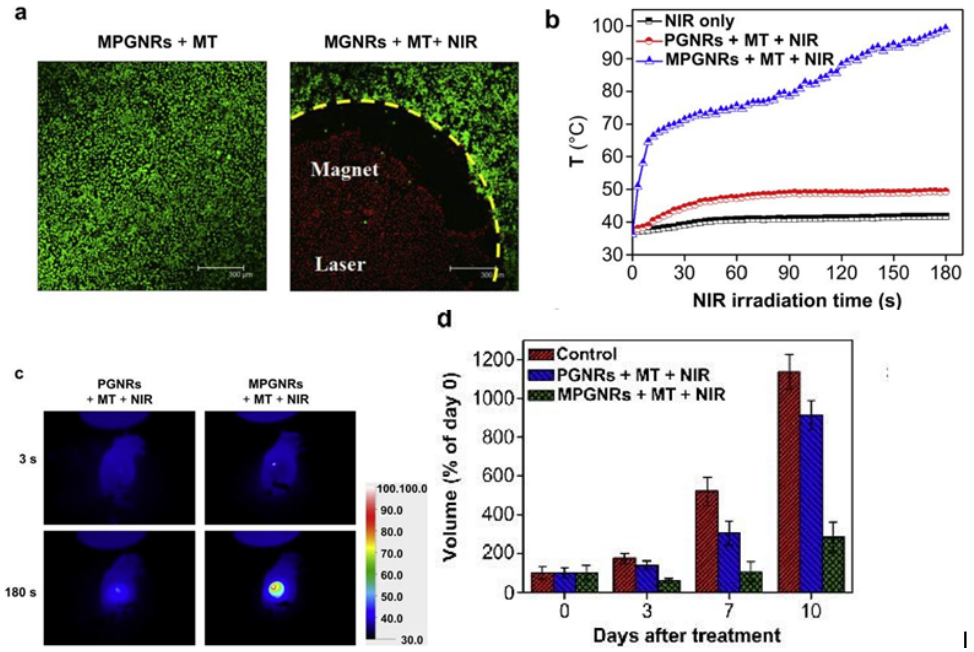

Figure 3: (a) The fluorescence C6 cell micrographs were subjected to 24 h in lower left of the yellow line and were treated with MPGNRs. They were subjected to a 900-Gauss magnet field. Left: in front of radiation. Right: after radiation (808 nm for 2 min; green: live cells, red: dead cells).

(b) Rise in temperature vs. time during irradiation. (c) The conversion of light absorption into heat by photothermal effect during irradiation for 3 min. (d) Quantitative study of the impact of different drugs on tumor size. Reprinted with the permission of Ref[18].

Multifunctionalized IONPs

The utilization of small molecules or biomolecular targeting, or therapeutic ligand (for example, Herceptin combined to MnFe2o4 nanoparticles) for molar specificity can be aimed against iron oxide nanoparticles. [13] The report [13] SPIONs are conjugated to target molecules to provide an appropriate concentration in the tumor region. Protein molecules were examined as carriers of medication, and may be appropriate diagnostic and treatment supplements for IONPs. IONPs have also been used to include different macromolecular drugs, including protein, peptide and DNA therapy [19].

Review of multifunctionalized IONPs based theranostic agents(Part A&B) Part(A)

A research by Daryoush Shahbazi and Mohammad Abdolahi was carried out in 2013, which combined with antibodies are applied as medicinal agents and have given tumor specific contrast increases for MRI with this study-specific agent(Nanomag-D-Superparamagnetic Iron Oxide (SPIO). In its analysis, the detection (MUC1)-expressing cancer of ovarian cancers using MRI maging was done using C595 monoclonal antibody (mAb) conjugated SPION (SPIONs-C595). (TEM images are seen in (Figure 4) in Nanomag-D-SPIO and SPION-C595) The MRI and anti-cancer parameters of their synthesis were investigated. After different incubation hours (2h, 8h, and 24h) at various iron concentrations for cell line, the in vitro cytotoxic effect of Nanomag-D-SPIO and the nanoprobe functionalized C595 mAb was investigated; more than 80% cell viability was reported in comparison to the power (Figure 5a).

Figure 4 TEM images for antibody binding decreases particle agglomeration significantly in (a) Nanomag- D-SPIO and (b) SPIONs-C595 TEM images. Particle sizes measured from TEM images ranged between 10 and 20 nanometers. With permission from Ref [18], this article has been reprinted.

The SPIONs-C595 was tested as a basic MR imaging agent, and the results showed that when compared to the Nanomag-D-SPIO, the SPIONs-C595 decreased 95 percent of the MR image signal

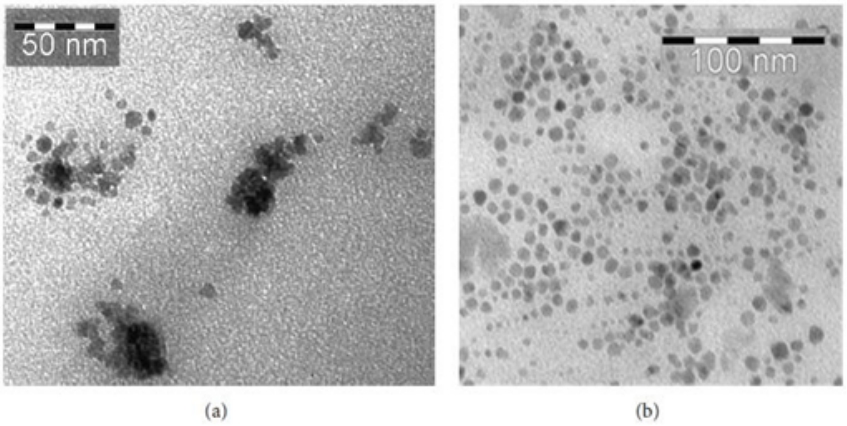

Figure 4: TEM images for antibody binding decreases particle agglomeration significantly in (a) Nanomag- D-SPIO and (b) SPIONs-C595 TEM images. Particle sizes measured from TEM images ranged between 10 and 20 nanometers.

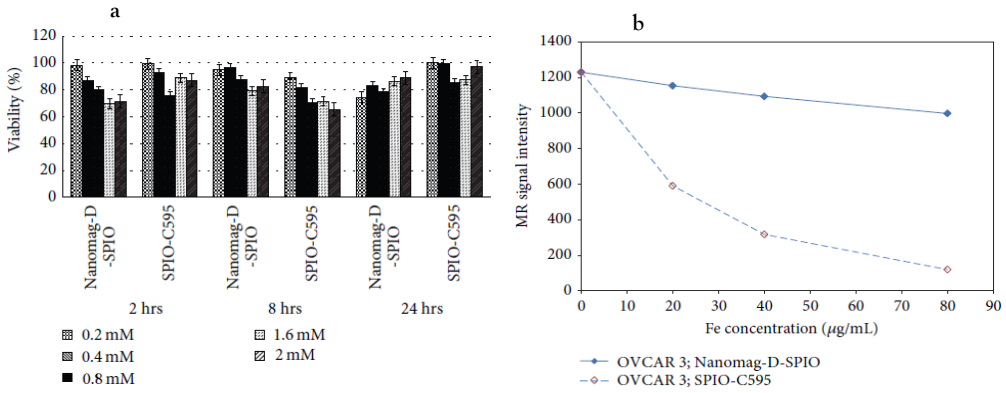

Figure 5: (a) Nanomag-D-SPIO and SPIONs-C595 in vitro cytotoxicity in the OVCAR3 cell line using the MTT assay with varying Fe concentrations ranging from 0.2 to 2.4mM for 2, 8, and 24 hours. (b) At separate Fe concentrations, the MR image signal voltage of both C595-SPIONs and Nanomag-D-SPIOs. With permission from Ref [20], this article has been reprinted.

amplitude in OVCAR3. (Figure 5b).

Figure 5a Nanomag-D-SPIO and SPIONs-C595 in vitro cytotoxicity in the OVCAR3 cell line using the MTT assay with varying Fe concentrations ranging from 0.2 to 2.4mM for 2, 8, and 24 hours (b) At separate Fe concentrations, the MR image signal voltage of both C595-SPIONs and Nanomag-D-SPIOs. With permission from Ref [20], this article has been reprinted.

Prussian blue staining assay was used to determine the specificity and cellular absorption of SPIONs- C595 and Nanomag-D-SPIO to the cells, and cells incubated with nonfunctionalized particles remained alive, as shown in (Figures 1 & 6).

Figure 6. Prussian blue staining images for OVCAR3 cells after 1 h incubation with (a) Nanomag-D-SPIO and (b) SPIONs-C595 nanoprobes (objective magnification: 40). With permission from Ref [20], this article has been reprinted.

T2 relaxation time affects MR signal strength, and SPIONs alter T2 values, lowering signal intensity. In vivo MR imaging revealed significant differences in signal intensities and T2 values of ovarian cancers after injection of SPIONs-C595 versus Nanomag-D-SPIO. (Images of mice before and after the presence of both non-functionalized and functionalized SIONPs were seen in MR images before and after the presence of the nanoprobe) (Figure 7) For SPIONs-C595 and Nanomag-D-SPIO, the signal amplitude reduction was 56 percent and 10%, respectively. The biodistribution of SPIONs-C595, Nanomag-D- SPIO, and regulation in tumors and other organs was determined using a Plasma Atomic Emission Spectroscopy (ICP-AES) assay (lung, heart, liver, spleen and

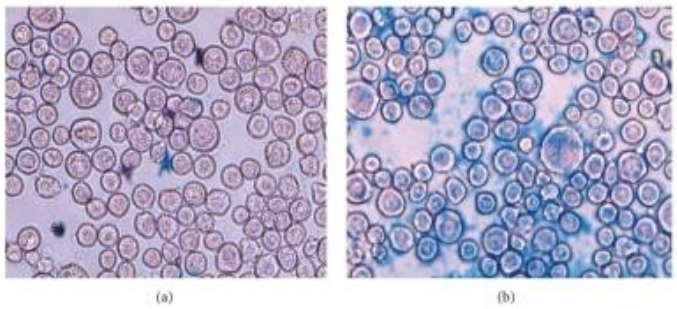

Figure 6: Prussian blue staining images for OVCAR3 cells after 1 h incubation with (a) Nanomag-D-SPIO and (b) SPIONs-C595 nanoprobes (objective magnification: 40).

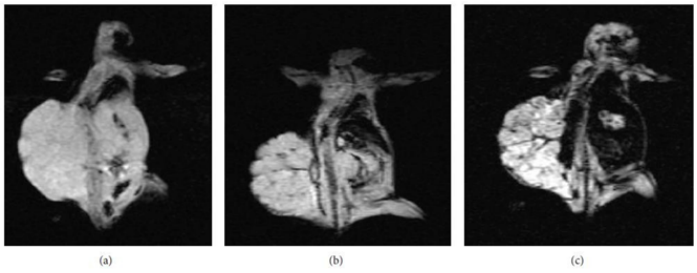

Figure 7: MR Image of mice: (a) Before the agents were injected. (b) after the Nanomag-D-SPIO was injected, and (c) after the C595-SPIONs were injected. With permission from Ref [20], this article has been reprinted.

kidney). The tumor uptaked SPIONs-C595 was around two times higher than the other organs in vivo, according to the findings. They found substantial tumor aggregation and diagnosis without in vivo toxicity as a result [20].

Figure 7. MR Image of mice: (a) Before the agents were injected, (b) after the Nanomag-D-SPIO was injected, and (c) after the C595-SPIONs were injected. With permission from Ref [20], this article has been reprinted.

Part (B)

Jin Xie et al used dopamine to alter the surface of IONPs, resulting in nanoconjugates that can easily be encapsulated into human serum albumin (HSA) matrices (clinically utilized drug carriers). The 64Cu- DOTA and Cy5.5 dyes were used to mark the HSA coated IONPs (HSA-IONPs). The multi-functional HSA-IONPs are schematically shown in (Figure 9a, and TEM effects are seen in (Figure 9b and c).

Figure 9a Schematic illustration of the multi-funtional HSA-IONPs. The pyrolysis-derived IONPs were incubated with dopamine, after which the particles became moderately hydrophilic and could be doped into HSA matrices in a way similar to drug loading. (b) TEM of oleate coated IONPs in hexane. (c) TEM of the HSA-IONPs in water. Reprinted with permission from Ref [21].

A subcutaneous U87MG xenograft mouse model was used to evaluate the multifunctional HSA-IONPs. PET/NIRF images were taken 1 hour, 4 hours, and 18 hours after the animal models were injected with HSA-IONPs. The contrast in both imaging methods changed over time, but PET imaging findings display much higher tumor/muscle ratios than NIRF results (Figure 10a and b). In a different technique, MRI images were collected before and 18 hours after injection (Figure 10c), and these tri-modality imaging were compared. The highlight features obtained by MRI were first, a high spatial resolution, and second, a clear definition of particle distribution pattern. However, the MRI system was found to be less sensitive than the other two methods. The other two approaches take care of this issue. PET is shown to have a higher signal-to-noise ratio than the other two approaches.

Figure 10.(a) In vivo NIRF images of a mouse that was injected with HSA-IONPs. Images were taken 1 hour, 4 hours, and 18 hours after injection. (b) Findings of of vivo PET imaging in mice injected with HSA-IONPs. Images were taken 1 hour, 4 hours, and 18 hours after injection. (c) MRI photographs taken before and 18 hours after the injection. With permission from Ref [19], this article has been reprinted.

The mice were sacrificed for this research, and in vitro PET/NIRF imaging of the tumor and main organs was performed (Figure 11).

The tumor tissue had the largest concentration of HSA-IONPs, followed by the liver organ, which had the second highest accumulation. NIRF also discovered a higher history.

Figure 11a PET imaging of the tumor and main organs ex vivo (b) NIRF imaging of the tumor and main organs in vivo. With permission from Ref [19], this article has been reprinted.

We concluded in this study that HSA, with its high binding capacity, plays an important role in theranostic applications [21].

Small interfering RNA (siRNA) could down regulate specific protein expression by suppressing a targeted gene selectively at the mRNA transcription level. Fe3O4 NPs are well-established depend on possess magnetic properties, actively investigated as

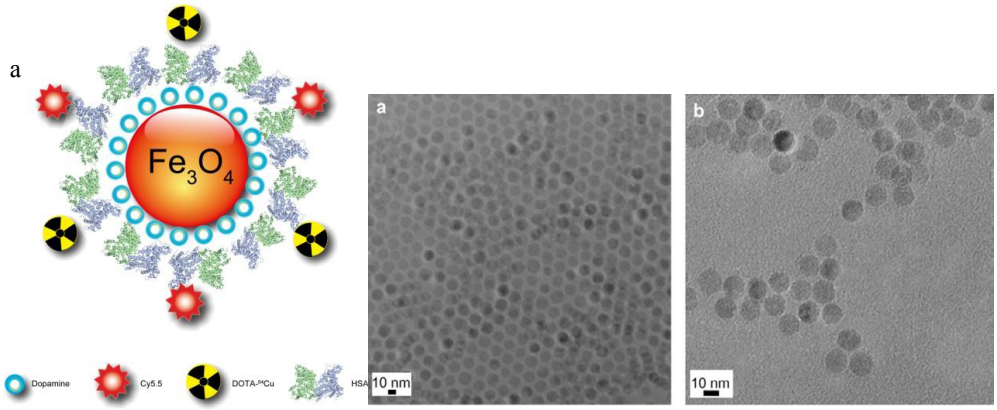

Figure 8: (a) Schematic illustration of the multi-funtional HSA-IONPs. The pyrolysis-derived IONPs were incubated with dopamine, after which the particles became moderately hydrophilic and could be doped into HSA matrices in a way similar to drug loading. (b) TEM of oleate coated IONPs in hexane. (c) TEM of the HSA-IONPs in water.

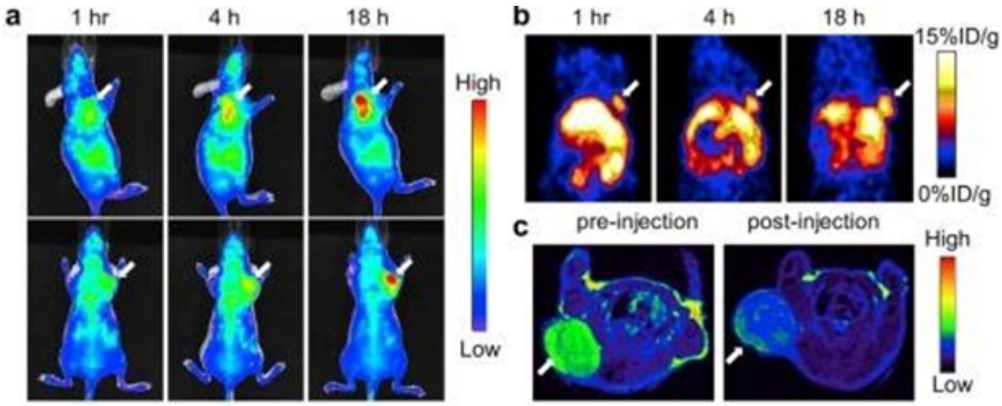

Figure 9: (a) In vivo NIRF images of a mouse that was injected with HSA-IONPs. Images were taken 1 hour, 4 hours, and 18 hours after injection. (b) Findings of of vivo PET imaging in mice injected with HSA-IONPs. Images were taken 1 hour, 4 hours, and 18 hours after injection. (c) MRI photographs taken before and 18 hours after the injection.

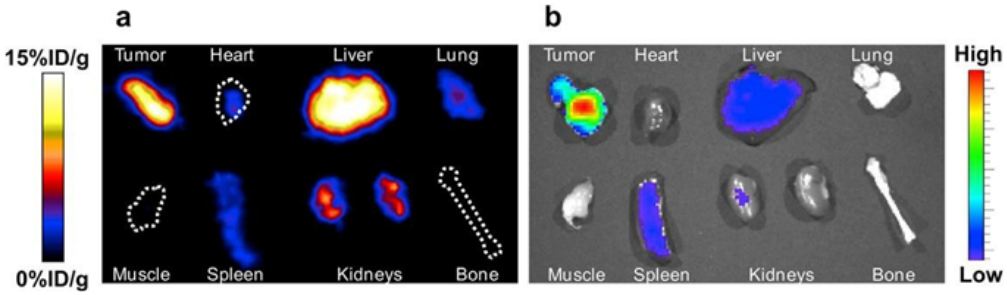

Figure 10: (a) PET imaging of the tumor and main organs ex vivo (b) NIRF imaging of the tumor and main organs in vivo. With permission from Ref [19], this article has been reprinted.

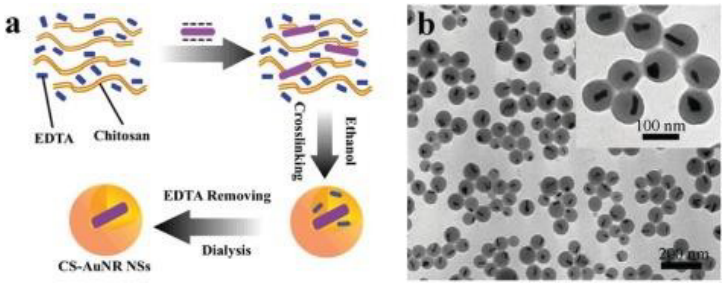

Figure 11: (a) Schematic Structure of CS-AuNR NSs; (b) TEM image of CS-AuNR NSs.

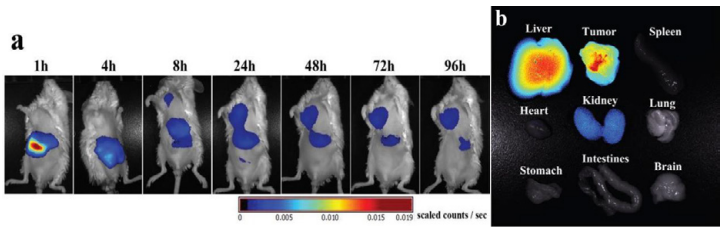

Figure 12: (a) NIR images of tumor-bearing mice after IV injection of NIR797 labelled CS-AuNR NSs; (b) fluorescence imaging of different organs 96 hours later.

new generation for MRI, excellent biocompatibility and versatile surface functionalization capability. Chen et al. [9] reported a multifunctional nanoclusters as an agent for dual-modal T1-T2 MRI imaging and siRNA delivery. Nanoclusters were self-assembled from the hydrophobic gadolinium (Gd) embedded Fe3O4 nanocrystals. The obtained GdIO-stPEI nanocluster showed good stability, dispersity and dual- modal MRI properties [9].

Properties of Gold nanoparticles(GNPs) as theranosticsagents

Gold NPs (GNPs) because its brilliant color and unique properties (e.g. fluorescence, photothermal, photoacoustic, low cytotoxicity, high quantum yields) by changing their shapes and sizes are highly appropriate for biomedical applications. [22,23] Actually they can effectively scatter incident light then convert it into heatin addition to they can increase the local electromagnetic fields near their surfaces [24].

Gold NPs (GNPs) are ideal for biomedical applications due to their bright color and peculiar properties (e.g. fluorescence, photothermal, photoacoustic, low cytotoxicity, high quantum yields) that can be changed by changing their shapes and sizes [22,23]. Really, they have the ability to disperse incident light and transform it to gas, as well as increase local electromagnetic fields near their surfaces [24].

Composite and multifunctionalized GNPs

Polymeric nanoparticles (e.g. poly (ethylene glycol), heparin, hyaluronic acid, chitosan, polystyrene sulfonate, polyethyleneimine, and xanthan gum) [25], other metal nanoparticles (e.g. Fe, Ag) [26-29], semiconductor nanoparticles, and dielectric nanoparticles could all be conjugated with gold nanoparticles (e.g. silica). This would increase the therapeutic efficacy of NPs as well as their stability. Gold nanoparticles' surfaces can also be conveniently adjusted for a particular use, and ligands for targeting, drugs contrast agents, therapeutic agents, and biocompatible coatings can all be added as multifunctional GNPs. As a result, by functionalizing these NPs with different molecules, we will increase their ability to accumulate on the disease. [30-32] The majority of the time, multifunctionalized GNPs were made by combining medications (e.g. DOX, Heparin, Antisense DNA) and attacking molecules (e.g. Biotin, Folic acid, Aptamer) [33-38].

A review of composite GNPs based theranosticagents

GNPs complexed with nanoparticles of the cationic biodegradable polyaminosaccharide chitosan are widely used (ChT). Chen R, et al. developed chitosan/gold nanorod hybrid nanospheres (CS-AuNR NSs) and ChT-coated gold nanorods doped with cisplatin (CS-AuNR-Pt NSs) (Figure 12). They looked at the clinical (drug delivery and PTT) and diagnostic (fluorescence imaging) aspects of CS-AuNR NSs in vitro and in vivo cases [39].

Figure 12a Schematic Structure of CS-AuNR NSs; (b) TEM image of CS-AuNR NSs. Reprinted with permission from Ref [39].

In vitro cytotoxicity studies

MTT assays were used to investigate the in vitro irradiation-

induced cytotoxicity of CS-AuNR NSs and CS-AuNR-Pt NSs on human cervical carcinoma (Hela cell). The experiment was carried out at various Au concentrations (5, 10, 20, 40, and 80 g mL-1) and with different NIR irradiation energy densities (No NIR, 2, 5 and 10 W Cm-1). They concluded that at varying concentrations of CS-AuNR NSs, cells did not exhibit any cytotoxicity without the intervention of NIR irradiation. Because of the chemical effects of cisplatin, CS-AuNR-Pt NSs showed cellular toxicity at elevated concentrations. However, cell viability of the Hela cell line was observed after co-incubation with CS-AuNR NSs and NIR light irradiation.

Without the assistance of NIR irradiation, the inhibition rate cells co-incubated with CS-AuNR-Pt NSs at a concentration of 20 gmL1 reached 19.1 percent. Cells co-incubated with CS-AuNR-Pt NSs and CS- AuNRNSs at the indicated concentrations with irradiation achieved inhibition rates of 59.2 percent and24.2 percent, respectively. As a result, gold nanorods were excellent photothermic transmutation products, and cisplatin had a strong synergistic effect with heat, increasing the number of dead cells at the same time [39].

In vivo biodistribution studies by NIR fluorescence imaging

CS-AuNR NSs is used as NIR photothermal agents in cancer therapy due to gold nanorodes' remarkable ability to transform NIR light into heat and ablate tumor tissues. Until investigating PTT in vivo, the biodistribution of CS-AuNR NSs was investigated. In tumor-bearing mice, the time-dependent localization and aggregation of CS-AuNR NSs were investigated. A near-infrared dye was labelled to CS- AuNR NSs for this purpose, and NIR fluorescence imaging was performed in vivo. The liver revealed a huge fluorescence signal in the first 4 hours after injection. A fluorescence signal of the CS-AuNR NSs was detected in the tumor tissue four hours after injection, and the signal became stronger and stronger over the next four hours (Figure 13a). At 96 hours after injection, the mice were sacrificed, and fluorescence imaging of different organs (spleen, breast, lung, stomach, brain, liver, intestines, kidney, and tumor) was performed. After 96 hours, the liver and tumor area had the largest concentration of CS- AuNR NSs, with minor concentrations in the kidneys (Figure 13b). The CS-AuNR NSs were not present in the otherorgans.

(a) NIR images of tumor-bearing mice after IV injection of NIR797 labelled CS-AuNR NSs;

(b) fluorescence imaging of different organs 96 hours later. With permission from Ref [37], this article has been reprinted.

In vivo photothermal conversion of nanocomposite

In order to study photothermal conversion of CS-AuNR NSs, the mice were split into two groups: one group of tumor-bearing mice was IV injected with saline, while the other group was intravenously injected with CS-AuNR NSs. At 8 hours after injection, the tumor regions of both classes were subjected to laser irradiation with a wavelength of 808 nm and a power density of 2 W cm2 for 10 minutes at an initial temperature of 28.2°C. After irradiation, the average temperature of the tumor for the classes of intravenously applied saline and CS-AuNR NSs reached 41.9°C and 49.0°C, respectively (Figure 14). This finding refers to the ability of gold nanoparticles to convert light to heat [39].

Figure 14. Infrared thermal images of the tumor in tumor bearing mice at different NIR laser irradiation times. Reprinted with permission from Ref. [39]

In vivo antitumor effects

H22 tumor-bearing mice were employed as the animal model to study in vivo antitumor effects. The mice were treated as follows: the first group received cisplatin-loaded CS-AuNR NSs with NIR irradiation (CS-AuNR-Pt (+)), the second group received cisplatin-loaded CS-AuNR NSs without irradiation (CS-AuNR-Pt (-)), the third group received CS-AuNR NSs with irradiation (CS-AuNR (+)), The saline (+) and CS-AuNR (-) classes had no effect on tumor development. The free Pt (-) group, on the other hand, exhibited antitumor activity due to their chemotherapy properties. The antitumor efficacy of the CS-AuNR-Pt (+) group was significantly higher than that of the free Pt (-) group. The CS-AuNR (+) and CS-AuNR-Pt (+) groups outperformed the others in terms of antitumor effectiveness. The mice in the CS-AuNR-Pt (+) group received chemo-photothermal therapy at the same time, but they were treated differently than the CS-AuNR (+) group. As a result, when PTT was used as an alternative solution, CS- AuNR-Pt improved the antitumor potency of the drug [39].

A review of multifunctional GNPs based theranosticagents

In one study a suitable efficacy was achieved by simultaneous attachment of DOX and biotin to GNRs (GNR/TSDOX) (Figure 15).

Figure 15a Schematic design of the multifunctional gold nanorods, (b) Characterization of the multifunctional gold nanorods. Reprinted with permission from Ref. [40].

In vitro thermo-chemotherapy effects of the multifunctional gold nanorod

On SCC-7 cancer cells and COS7 human cells, in vitro NIR-based thermotherapy and combinational thermo-chemotherapy of GNR/TSDOX and GNRs alone with or without NIR light irradiation (808 nm, 1 W cm2, and 1 min) were examined. The combination NIR-based thermo-chemotherapy of GNR/TSDOX resulted in much improved therapeutic results, with SCC-7 cancer

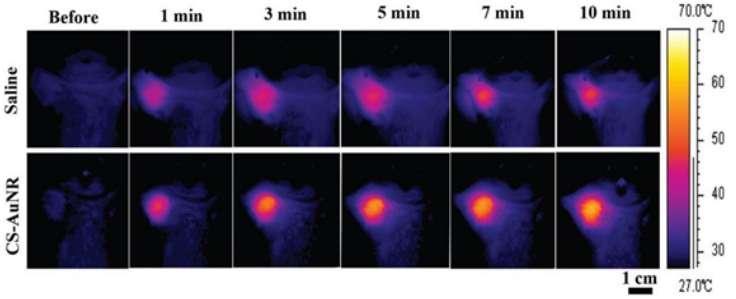

Figure 13: Infrared thermal images of the tumor in tumor bearing mice at different NIR laser irradiation times.

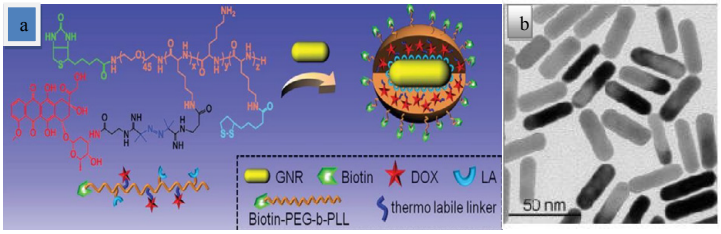

Figure 14: (a) Schematic design of the multifunctional gold nanorods, (b) Characterization of the multifunctional gold nanorods.

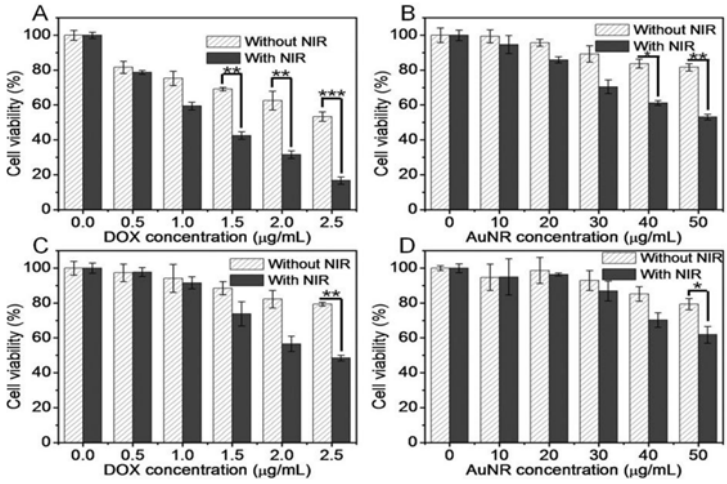

Figure 15: (A) SCC-7 cancer cells infected with GNR/TSDOX without or with NIR light irradiation had a higher relative viability (808 nm, 1 W cm^{-2}, 1 min). (B) SCC-7 cancer cells treated with GNRs without or with NIR light irradiation (808 nm, 1 W cm^2, and 1 min). (C) COS7 normal cells treated with GNR/TSDOX without or with NIR light irradiation (808 nm, 1 W cm^2, and 1 min) had a higher relative viability. (D)COS7 normal cells treated with GNRs without or with NIR light irradiation (808 nm, 1Wcm^2, and 1 min) had a higher relative viability. With permission from Ref. [38], this article has been reprinted.

cell viability reduced to 16 percent and COS7 natural cell viability reduced to 50 percent (Figure 16).

Figure 16. (A) SCC-7 cancer cells infected with GNR/TSDOX without or with NIR light irradiation had a higher relative viability (808 nm, 1 W cm^{-2}, 1 min). (B) SCC-7 cancer cells treated with GNRs without or with NIR light irradiation (808 nm, 1 W cm^2, and 1 min). (C) COS7 normal cells treated with GNR/TSDOX without or with NIR light irradiation (808 nm, 1 W cm2, and 1 min) had a higher relative viability. (D) COS7 normal cells treated with GNRs without or with NIR light irradiation (808 nm, 1 Wcm^2, and 1 min) had a higher relative viability. With permission from Ref. [38], this article has been reprinted.

In addition, images from the live/dead cell assay of SCC-7 cancer cells incubated with GNR/TSDOX were captured using confocal laser scanning microscopy (CLSM). Most cancer cells died as a result of this procedure when exposed to NIR light for 8 minutes, while COS7 regular cells remained intact (Figure 17).

Figure 17a CLSM images of SCC-7 cancer cells in a live/dead cell assay. The live and dead cells are represented by green and red dots, respectively (a). SCC-7 cancer cells were incubated with GNR/TSDOX for 12 hours without being exposed to NIR light. (b.) SCC-7 cancer cells were incubated with GNR/TSDOX for 12 hours and then exposed to NIR light for 8 minutes (808 nm, 1 W cm^2, 1 min). With permission from Ref. [40], this article has been reprinted.

In vivo Diagnostic modality (PT/PA imaging) of the multifunctional goldnanorods

GNR/TSDOX was administered intravenously to SCC-7 tumor-bearing mice as a diagnostic modality (PT/PA imaging). The blank power consisted of an intravenous infusion of PBS. Since receiving an intravenous injection of GNR/TSDOX, the SCC-7 tumor-bearing mice were exposed to an 808-nm laser for 3 minutes. Thermal images of SCC-7 tumor-bearing mice showed that the temperature of the local tumor rapidly increased. The tumor temperature was estimated at 44.1°C 2 hours after IV injection of GNR/TSDOX, which was adequate to kill cancer cells. The PBS injection, on the other hand, did not produce the desired temperature increase. Since biotin was introduced into the GNR/TSDOX IV injection, GNR/TSDOX accumulated selectively at the tumor site (EPR effect and active-targeting effect of biotin), and GNRs produced plasmonic heat for PTT after laser irradiation. This GNR/TSDOX property resulted in a significant PA imaging contrast effect. In

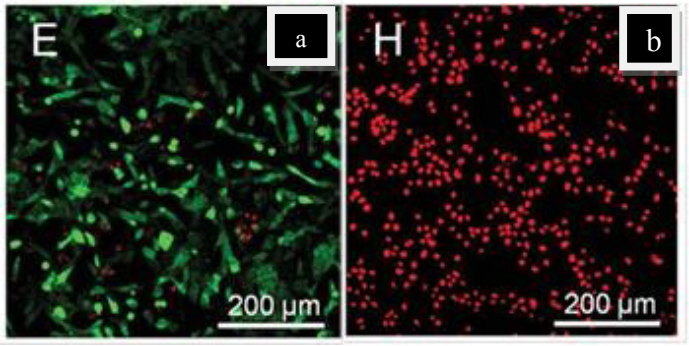

Figure 16: (a) CLSM images of SCC-7 cancer cells in a live/dead cell assay. The live and dead cells are represented by green and red dots, respectively (a). SCC-7 cancer cells were incubated with GNR/TSDOX for 12 hours without being exposed to NIR light. (b.) SCC-7 cancer cells were incubated with GNR/TSDOX for 12 hours and then exposed to NIR light for 8 minutes (808 nm, 1 W cm^2, 1 min).

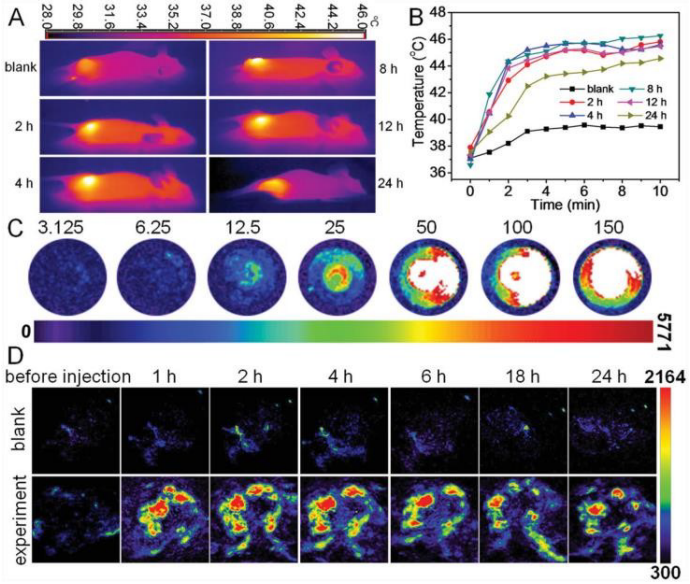

Figure 17: (a) Thermal images of SCC-7 tumor-bearing mice exposed to an 808-nm laser after intravenous injections of GNR/TSDOX at the specified time points, with a PBS injection as a blank control. (b) Temperature difference curve in tumor tissues as a result of irradiation time after laser irradiation. (c) GNR/TSDOX PA signals in vitro at various concentrations. (d) GNR/TSDOX photoacoustic imaging in tumor sites at various times, with PBS injection as a blank monitor.

this analysis, there was no discernible temperature increase in the mice's healthy tissues, which was a positive outcome (Figure 18).

Figure 18a Thermal images of SCC-7 tumor-bearing mice exposed to an 808-nm laser after intravenous injections of GNR/TSDOX at the specified time points, with a PBS injection as a blank control. (b) Temperature difference curve in tumor tissues as a result of irradiation time after laser irradiation. (c) GNR/TSDOX PA signals in vitro at various concentrations. (d) GNR/TSDOX photoacoustic imaging in tumor sites at various times, with PBS injection as a blank monitor. With permission from Ref. [40], this article has been reprinted.

SCC-7 tumor-bearing mice were sacrificed 1 hour, 12 hours, and 24 hours after receiving GNR/TSDOX via intravenous injection. The biodistribution of GNR/TSDOX in various organs (heart, liver, spleen, lung, and kidney) was then determined using ICP-MS analysis after systemic administration at 1 hour, 12 hour, and 24 hour intervals. The concentration of GNR/TSDOX in the tumor tissue increased over time. PBS, free DOX, GNR without NIR laser, GNR/TSDOX without NIR laser, GNR with NIR laser, GNR/TSDOX with NIR laser, and GNR/TSDOX with NIR laser were given to the sick mice in six categories. Because of therapeutic modality platforms for cancer care by integrating dual drug delivery/PT therapy, tumor development stopped roughly in GNR/TSDOX with NIR laser treatment, and tumor weights decreased in unhealthy mice after GNR/TSDOX with NIR laser treatment more than other treatments [40].

CONCLUSION

We describe the most representative advances in the field of nanotheranostics in this study, which discuss early detection and treatment of superficial and solid tumors. In order to reduce the time between regulatory clearance and therapeutic translation of these nanotechnologies, there is a strong emphasis on developing multifunctional theranostic nanoplatforms that include targeting molecules, photosensitizers, and anticancer drugs in clinical use. When compared to drugs that have been in commercial use for a long time, such as Doxil TM/Caelyx TM or Abraxane TM, nanotheranostics only have a small presence in clinical trials. The majority of the challenges derive from the complexities and synergistic results that arise from the combination of therapeutic and imaging modalities, as well as materials like those used in multifunctional hybrid nanosystems [41].

Major concerns are now focused on the optimization of tumor accumulation/retention and biodistribution of nanoparticles and delivered drugs by imaging techniques. Nanotheranostics may offer the right drug with the right dose to the right patient at the right time. Bright future for polymeric, metallic, and lipid- based nanosystems combining diagnostic and therapeutic functions is expected. Non-invasive imaging techniques are strongly needed to assess specificity receptor binding and internalization mechanisms in cancer cells. The interest of pharmaceutical companies to conduct clinical trials and further introduce novel nanotheranostic into the market will be crucial for the success of this research.

REFERENCES

1. Prashant K Jain, Xiaohua Huang, Ivan H EL-Sayed, Mostafa A EL-sayed. Noble Metals on the Nanoscale: optical and photothermal properties and some applications in Imaging, Sensing, Biology, and Medicine. Acc Chem Res. 2008;1578-1586 Vol. 41. No.12.
2. Paul Alivisatos. The use of nanocrystals in biological detection. Nat Biotechnol. 2004, Vol. 22 No. 1.
3. Etienne Duguet, SebastienVasseur, Stephane Mornet, Jean-Marie Devoisselle. magnetic nanoparticles and their application in medicine. Nanomed. 2006;1(2).157-168.
4. Nasongkla N, Bey E, Ren J, Ai H, Khemtong C et al. Multifunctional polymeric micelles as cancer-targeted, MRI-ultrasensitive drug delivery systems. Nano Lett. 2006;6:2427–2430.
5. Xiaohua Huang. Gold nanoparticles used in cancer cell diagnostics, selective photothermal therapy and catalysis of NADH oxidation reaction. Georgia Inst ofTechnolog.2006.
6. Zhao Peng, Chenxiao Wang, Erhu Fang, Xiaoming Lu, Guobin Wang, et al. Co-Delivery of Doxorubicin and SATB1 shRNA by thermosensitive magnetic cationic liposomes for gastric cancer therapy, PLOS ONE. 2014;9.
7. Skeel RT, Khleif SN.Handbook of cancer chemotherapy edited by Lippincott Williams and Wilkins, Philadelphia. 2011.
8. Lilianne Beola, Valeria Grazú, Yilian Fernández-Afonso, Raluca M. Fratila, Marcelo de las Heras et al. ACS Appl Mater Interfaces. 2021;13(11),12982-12996.
9. Zhao S, Yu X, Qian Y, Chen W, Shen J et al. Multifunctional magnetic iron oxide nanoparticles: an advanced platform for cancer theranostics. Theranostics. 2020;10(14):6278-6309.
10. Jesse V. Jokerst, Sanjlv S. Gamblir. Molecular imaging with theranostic nanoparticles. Acc Chem Res. 2011;1050–1060.10.
11. Chouly C, Pouliquen D, Lucet I, Jeune J.J, Jallet P. Development of superparamagnetic nanoparticles for MRI: effect of particle size, charge andsurfacenature on biodistribution. J. Microencapsul. 1996;(13)245–255.
12. Grancharov S.G, Zeng H, Sun S.H, Wang S.X, Brien S.O et al. Bio-functionalization of monodisperse magnetic nanoparticles and their use as biomolecular labels in a magnetic tunnel junction based sensor, J.Phys. Chem. B. 2005;13030-13035.

13. Jae-Hyun Lee, Yong-Min Huh. Yong-Wook Jun, Jung- WookSeo, Jung-tak Jan et al. Artificially engineered magnetic nanoparticles for ultra-sensitive molecular imaging. Nat Med. 2007;13:1.

14. Jin Xie, Seulki Lee, Xiaoyuan Chen. Nanoparticle-based theranostic agents.Adv. Drug Deliv Rev. 2010;1064-1079.

15. JihRuHwu, Yu Sern Lin, ThainashmuthuJ, Ming-Hua Hsu, Fong-Yu Cheng et al. Targeted paclitaxel by conjugation to iron oxide and gold nanoparticles. J AM CHEMSOC. 2009;131.

16. Wu C-H, Cook J, Emelianov S. Multimodal magneto-plasmonicnanoclusters for Biomedical applications. AdvFunct Mater. 2014;24,6862–6871.

17. Chatterjee, D.K. Nanoparticle-mediated hyperthermia in cancer therapy. Ther. Deliv. 2011;2,1001–1014.

18. Yang HW, Liu HL, Li ML. Magnetic gold-nanorod/PNIPAAmMA nanoparticles for Dual magnetic resonance and photoacostic imaging and targetedphotothermalTherapy. Biomat. 2013; (34):5651e5660.

19. Harshita Sharma, Pawan K. Mishra. Metal nanoparticles: a theranostic nanotool Against cancer. Drug Discov Today. 2015;20(9):1143-51.

20. Shahbazi-Gahrouei, D, Abdolahi, M. Detection of MUC1-expressing ovariancancer by C595 monoclonal antibody-conjugated SPIONs using MR imaging. Sci. World J. 2013;609151.

21. J. Xie, K. Chen, J. Huang, S. Lee, J. Wang et al. Triplefunctional iron oxide nanoparticles, Biomaterials, 2010;13.123016-3022.

22. Khan, M.S. Gold nanoparticles: a paradigm shift in biomedical application Adv. Colloid. Interface Sci. 2013;199.44–58.

23. Hong Liang, HuayuTian, Mingxiao Deng, Xuesi Chenb. Gold nanoparticles for cancer theranostics. Chin. J. Chem. 2015;33,1001-1010.

24. Lev A. Dykman, Nikolai G. Khlebtsov, Multifunctional gold-based nanocomposites for theranostics. Biomaterials.2016;108:13-34.

25. Omkara Swami Muddineti, Balaram Ghosh, Swati Biswas. Current trends in using polymer coated gold nanoparticles for cancer therapy. Int. J. Pharm.2015;30,484(1-2):252-67.

26. SujataPatra, Sudip Mukherjee. Green synthesis characterization of gold and silver nanoparticles and their potential application for cancer therapeutics. Mater. Sci. Eng. C. 2015;53.298–309.

27. Mohammad F, Balaji G, Weber A, Uppu RM, Kumar CS. Influence of gold nanoshell on hyperthermia of superparamagnetic iron oxide nanoparticles (SPIONs). J. Phys. Chem. C Nanomater. Interfaces 2010;1.(20): 3141–3146.

28. J Ghanavi, M Mostafavi, Z Ghanavi. Method for the synthesis of metallic nanoproducts.US Patent 9,487,399, 2016.

29. J Ghanavi and M Mostafavi. Method for producing rod-shaped and branched metallic nano-structures bypolyol compounds - US Patent20110088511.

30. Sapsford KE, Algar WR, Berti L.Functionalizing nanoparticles with biological molecules: developing chemistries that facilitate nanotechnology. Chem Rev. 2013;(13):1904- 2074.

31. Jiao PF, Zhou HY, Chen LX et al. Cancer-targeting multifunctionalized gold nanoparticles in imaging and therapy. Curr Med Chem. 2011;(18):2086-102.

32. Aneta J. Mieszawska, Willem J. M. Mulder.Multifunctional Gold Nanoparticles for Diagnosis and Therapy of Disease. Mol Pharm. 2013;10(3):831-47.

33. Mukherjee P, Bhattacharya R, Mukhopadhyay D. Gold nanoparticles bearing functional anti- cancerdrug and anti-angiogenic agent: a “2 in 1”system with potential application in cancer therapeutics. JBiomed Nanotech. 2005;(1):224-8.

34. Heo DN, Yang DH, Moon H-J, et al. Gold nanoparticles surface-functionalized with paclitaxel drug and biotin receptor as theranostic agents for cancer therapy. Biomaterials. 2012;33:856-66.

35. Book Newell B, Wang Y, Irudayaraj J. Multifunctional gold nanorodtheragnosticsprobedby multiphoton imaging. Eur J Med Chem. 2012;48:330-7.

36. Kim D, Jeong YY, Jon S. A drug-loaded aptamer-gold nanoparticle bioconjugate for combined CT imaging and therapy of prostate cancer. ACS Nano. 2010;4:3689-96.

37. Lee K, Lee H, Bae KH. Heparin immobilized gold nanoparticles for targeteddetection andapoptotic death of metastatic cancer cells. Biomaterials. 2010;31:6530-6.

38. Bao C, Conde J, Curtin J. Bioresponsive antisense DNA gold nanobeaconsasa hybrid in vivo theranostics platform for the inhibition of cancer cells andmetastasis. Sci Rep. 2015;(5):12297.

39. Chen R, Zheng X, Qian H. Combined near-IR photothermal therapy and chemotherapy using goldnanorod/chitosan hybrid nanospheres to enhance the antitumor effect. Biomater Sci. 2013;(3):285-93.

40. Chen W-H, Yang C-X, Qiu W-X. Multifunctional theranostic nanoplatform for cancer combined therapy based on gold nanorods. AdvHealthc Mater 2015;4:2247-59.

41. Silva CO, Pinho JO, Lopes JM, Almeida AJ, Gaspar, MM et al. Current Trendsin Cancer Nanotheranostics: Metallic, Polymeric, andLipid-BasedSystems. Pharmaceutics 2019;11-2.